Electronic Supporting Information

for

Polyoxometalate derived bimetallic phosphides electrocatalyst for high-efficiency hydrogen evolution reactions

Yunxiu Zhao,[a] Jinghong Wen,[a] Ping Li,[a] Yang Xiang,[a] Meiqi Li,[a] Suna Wang,[a] Jianmin Dou,[a] Yunwu Li,[*a,c] Huiyan Ma,[*a,c] and Liqiang Xu[*b]

[a]Shandong Provincial Key Laboratory of Chemical Energy Storage and Novel Cell Technology, School of Chemistry and Chemical Engineering, Liaocheng University, 252000 P. R., China.

[b]Key Laboratory of Colloid and Interface Chemistry, Ministry of Education, School of Chemistry and Chemical Engineering, Shandong University, Jinan 250100 P. R., China.

[c]Key Laboratory of Advanced Energy Materials Chemistry (Ministry of Education), Nankai University, Tianjin 300071 P. R., China.

Corresponding authors.

E-mail addresses: liyunwu@lcu.edu.cn; mahuiyanyan@163.com; xulq@sdu.edu.cn.

Contents

S1. Experimental Section

S1.1. Chemicals

All reagents are analytical grade and used as received.

S1.2. Material characterization

The crystallographic data of $[Ni(2,2'\text{-bipy})_3][Mo_6O_{19}]$ precursor were collected on a Bruker SMART at 298(2) K with Mo-*K*α radiation (λ = 0.71073 Å). The powder X-ray diffraction (PXRD) was obtained on a D/MAX-rA (Rigaku) diffractometer with Cu *K*α radiation (λ = 1.542 Å) with a scan rate of 4° min^{-1}. Raman spectrum was tested using Monovista CRS500. X-ray photoelectron spectrums (XPS) were carried out using ESCALAB Xi+. Electron microscopy measurements were measured using field-emission scanning electron microscopy (SEM, JSM-6360). Transmission electron microscopy (TEM) was measured by JEM-2100 at 200 kV.

S1.3. Syntheses of $[Ni(2,2'\text{-bipy})_3][Mo_6O_{19}]$

The mixture of $Ni(NO_3)_2{\cdot}6H_2O$ (0.20 mmol, 0.0582 g), $(NH_4)_6Mo_7O_{24}{\cdot}4H_2O$ (0.20 mmol, 0.2472 g), 2,2'-bipy (0.3 mmol, 0.0468 g), and ultrapure water (12 mL) was sealed in a Teflon-lined autoclave and heated at 160 °C for 3 days, then slowly cooled to room temperature. After being washed with H_2O three times, parallelogram block like orange crystals of $[Ni(2,2'\text{-bipy})_3][Mo_6O_{19}]$ were harvested in 45% yield based on Mo. The detailed crystal data see **Table S1** in **ESI**.

S1.4. Syntheses of MoP/MoNiP@NPC series catalysts

A certain amount of $[Ni(2,2'\text{-bipy})_3][Mo_6O_{19}]$ and $NaH_2PO_2{\cdot}H_2O$ (mass ratio 1:10) were loaded into a porcelain boat, in which $[Ni(2,2'\text{-bipy})_3][Mo_6O_{19}]$ was placed downstream of the N_2 flow as a metal source, a nitrogen source and also a carbon source, while $NaH_2PO_2{\cdot}H_2O$ was placed upstream as a phosphorus source. Then heated at a rate of 5 °C·min^{-1} in N_2 atmosphere and calcined at different temperatures (700~850 °C, respectively) for 2 h. The collected black products were crushed, acidified with 3.0 M hydrochloric acid solution, washed five times with ultrapure water and ethanol and dried at 60 °C, centrifuged to collect the final black powder, which are represented by **POM**-x (x represents calcined temperature).

Finally, for comparison, the single-component **Ni-POM** crystals were also

calcined at 800 °C to remove phosphating effect by without adding NaH_2PO_2 source, and the product is abbreviated as **POM(S)**-800.

S1.5. X-ray crystallography

The X-ray single crystal diffraction (XRSCD) of $[Ni(2,2'\text{-bipy})_3][Mo_6O_{19}]$ was collected by Mo-*K*α radiation (λ = 0.71073 Å) on a Bruker SMART diffractometer at 298(2) K. The crystal data was solved by direct methods and refined by a full-matrix least-square method on F^2 using *SHELXL-97* crystallography software package.[S1] Mo and Ni atoms in $[Ni(2,2'\text{-bipy})_3][Mo_6O_{19}]$ were found from *E*-maps and other non-hydrogen atoms were located in successive difference Fourier syntheses. The final refinement was performed by full matrix least-squares methods with anisotropic thermal parameters for non-hydrogen atoms on F^2. The hydrogen atoms of organic ligands were added theoretically, riding on the concerned atoms and refined with fixed thermal factors. During the refinement, the command "omit -3 50.02" was used to omit some disagreeable reflections. Further details of crystal data and structure refinement for $[Ni(2,2'\text{-bipy})_3][Mo_6O_{19}]$ were summarized in **Table S1** (**ESI**).

S1.6. Electrochemical measurements

The electrocatalytic properties were carried out using Gamry references 3000 electrochemical workstations, equipped with an electrode rotator (Pine, RDE710). A typical experiment: 2.5 mg MoP/MoNiP@NPC-800 catalyst (or 20% Pt/C) was dispersed in a mixture of 570 μL ultra-pure H_2O and 177 μL ethanol under supersound, and 3 μL 5 wt.% Nafion was added. Then, 10.0 μL catalyst ink was dropped on the glassy carbon rotating disk electrode (RDE, 0.196 cm^2) and air dried. So both of the mass loading of the MoP/MoNiP@NPC-800 catalyst and Pt/C catalyst on the electrodes is 0.17 mg cm^{-2}. A three-electrode cell system was worked in 70 mL electrolyte.

In this work, 0.5 M H_2SO_4 and 1.0 M KOH was used as acid and alkaline electrolyte, respectively. The electrolyte was treated with nitrogen before the polarization curve was measured. The working electrode is RDE (rotating disk electrode) glassy carbon, the counter electrode is graphite rod, the reference electrode is Hg/HgO in 1.0 KOH electrolyte and Hg/Hg_2SO_4 in 0.5 M H_2SO_4. The catalytic

performance of the catalyst was evaluated mainly by linear sweep voltammetry (LSV) with a scan rate of 5 mV s^{-1}. Significantly, all the potentials were calibrated in regard to a reversible hydrogen electrode (RHE) on the basis of $E_{(RHE)} = E_{(Hg/HgO)} + 0.059pH + 0.098$ and $E_{(RHE)} = E_{(Hg/Hg_2SO_4)} + 0.059pH + 0.652$ in 1.0 M KOH and 0.5 M H_2SO_4, respectively. Furthermore, all Tafel plots are according to the equation: $\eta = a + b\log|j|$ according to the LSV curves, herein, η is the overpotential, a is the exchange current density, b is the Tafel slope, and j is the current density. Double-layer capacitance (C_{dl}) values were obtained *via* cyclic voltammetry (CV) tests with the scan rates of 10, 20, 40, 60, 80, 100, 120, 140, 160 and 180 mV s^{-1}. Electrochemical impedance spectroscopy (EIS) measurements were proceeded with specific voltage ranged from 0.1 to 100000 Hz. Stability tests were performed in both acidic and alkaline solutions *via* 1000 CV cycles and *V-t* curves.

S1.7. Density functional theory (DFT) calculations

DFT calculations were performed using the plane-wave approach with the projector-augmented wave (PAW) method implemented in the Vienna Ab Initio Simulation Package (VASP).[S2-S4] The Perdew-Burke-Ernzerhof (PBE) exchange correlation functional was used.[S5] The kinetic energy cutoff for the plane-wave basis set was 400 eV, and a Brillouin zone sampling of 1 × 1 × 1 k-points was used for MoP (101) and MoNiP (111), and 3 × 3 × 1 k-points was used for MoP@NPC and MoNiP@NPC.

S2. Additional Figures

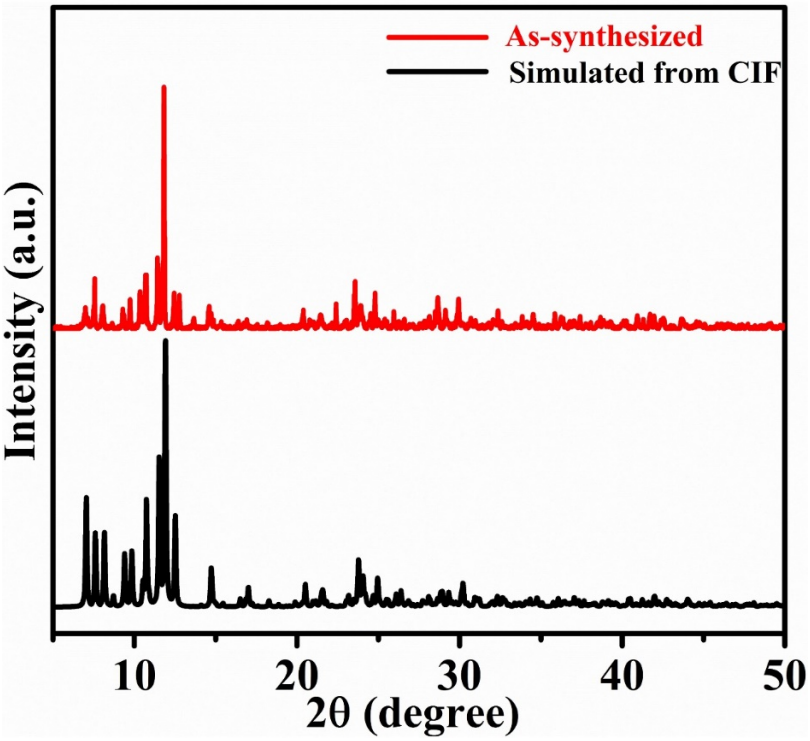

Fig. S1. PXRD patterns of **Ni-POM** precursor. (Black: Simulated, Red: As-synthesized).

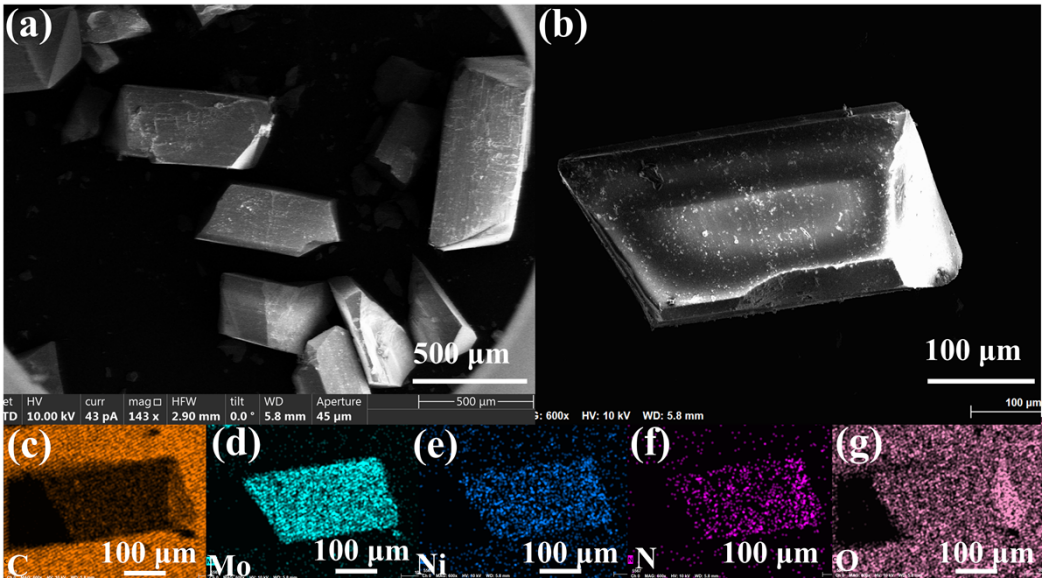

Fig. S2. (a,b) The SEM images of different magnifications and (c-g) the EDS mapping images of selected regions: Mo, Ni, C, N and O for **Ni-POM** precursor.

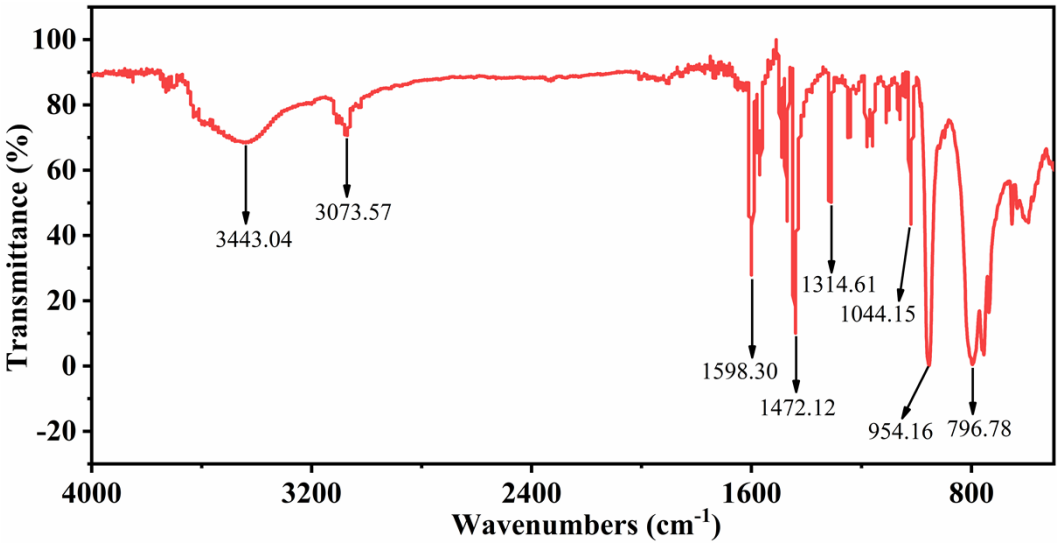

Fig. S3. IR patterns of **Ni-POM** precursor.

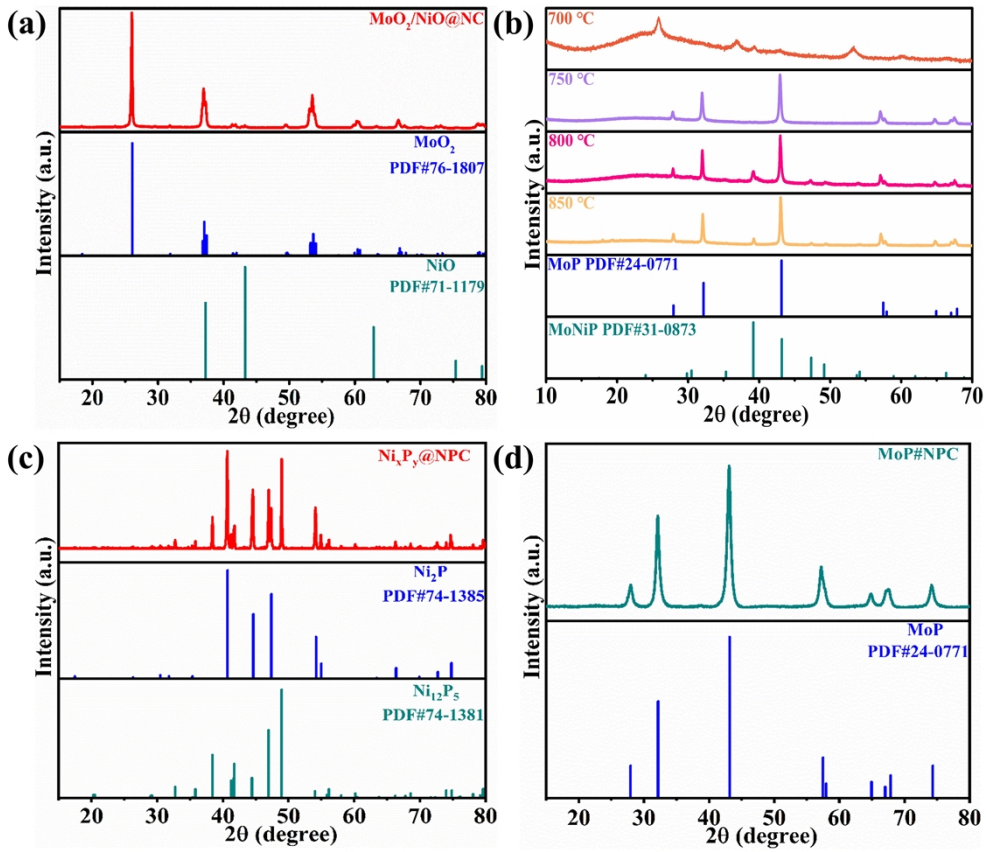

Fig. S4. PXRD patterns of (a) **POM(S)**-800. (b) **POM**-700, **POM**-750, **POM**-800 and **POM**-850. (c) Ni_xP_y@NPC and (d) MoP@NPC.

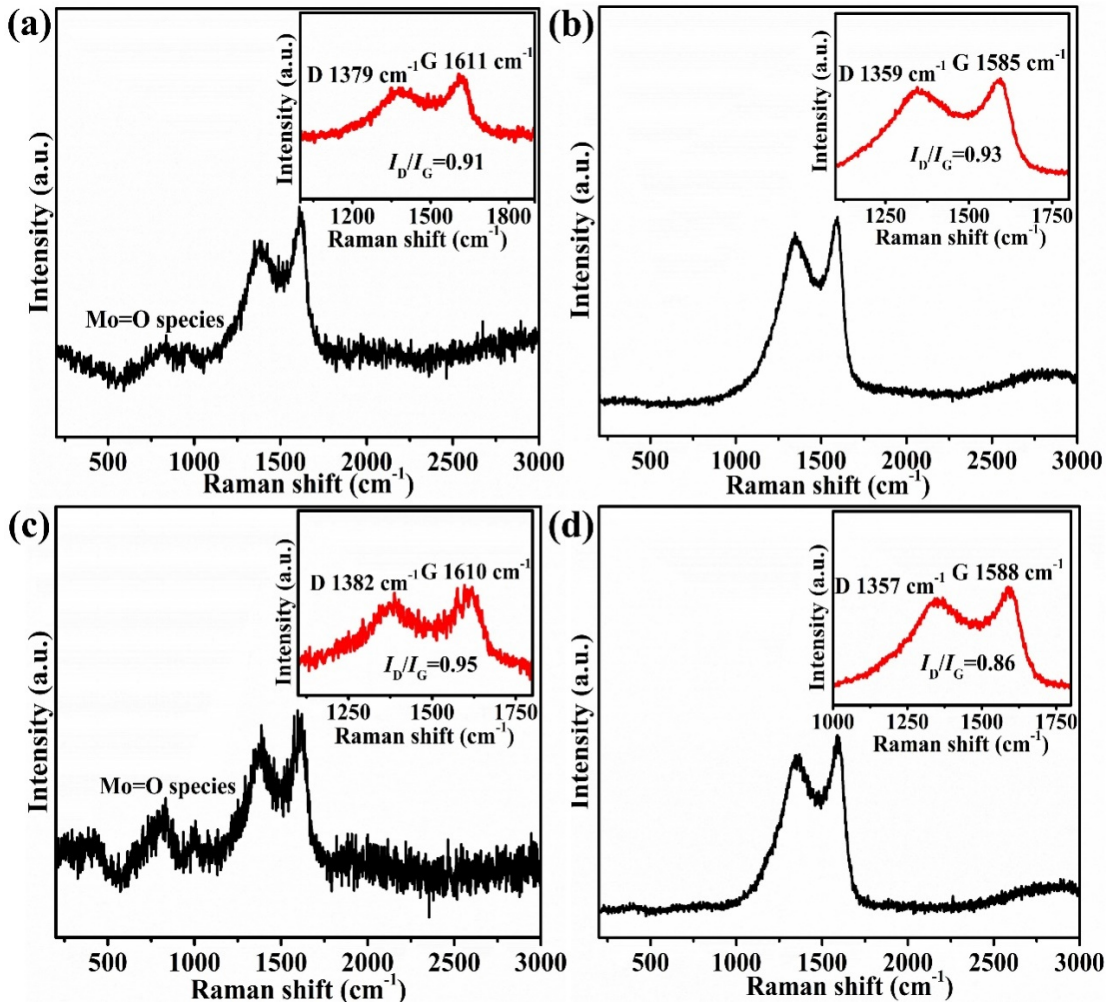

Fig. S5. Raman patterns of (a) **POM**-700. (b) **POM**-750. (c) **POM**-850 and (d) **POM(S)**-800.

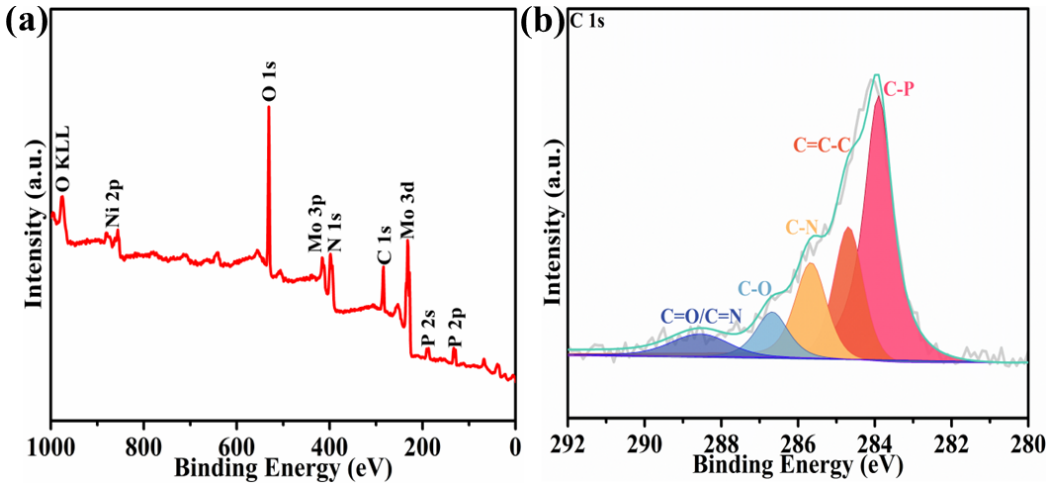

Fig. S6. (a) The XPS survey spectrum and (b) High-resolution XPS: C 1s.

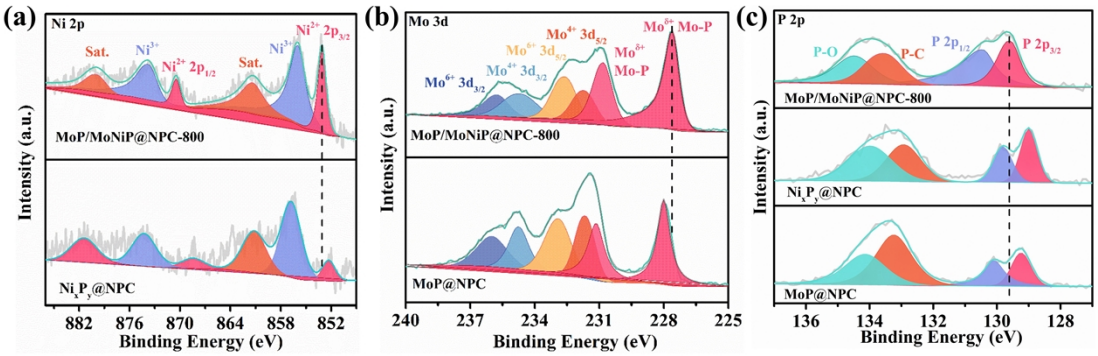

Fig. S7. High-resolution XPS spectra. (a) Ni 2p of MoP/MoNiP@NPC-800 and Ni_xP_y@NPC. (b) Mo 3d of MoP/MoNiP@NPC-800 and MoP@NPC. (c) P 2p of MoP/MoNiP@NPC-800, Ni_xP_y@NPC and MoP@NPC.

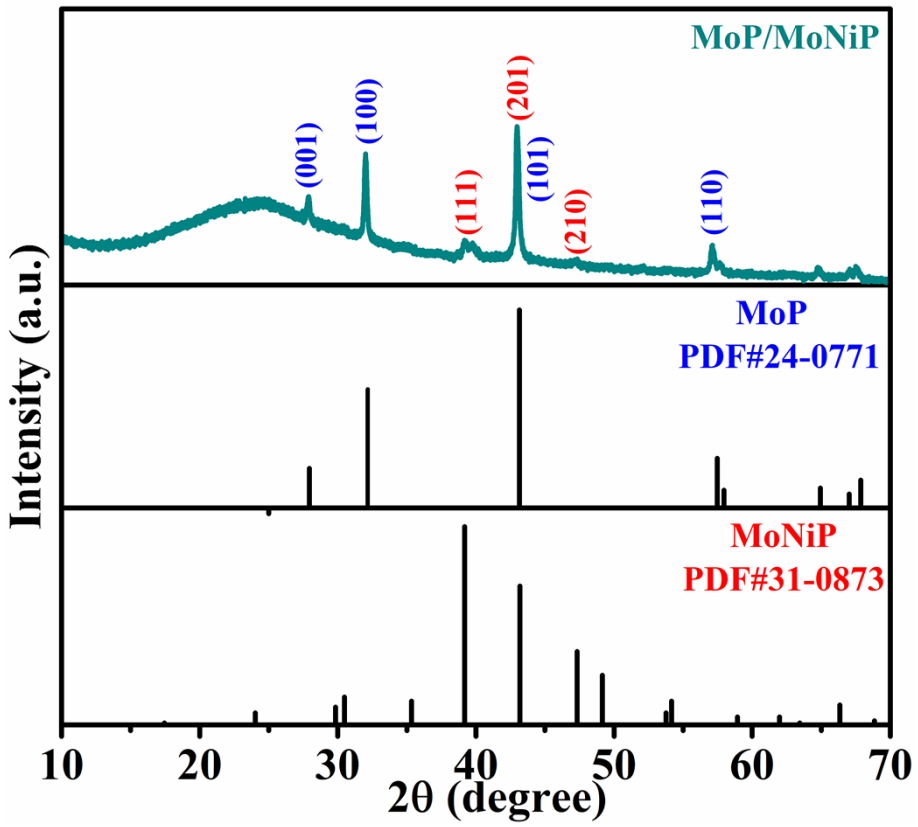

Fig. S8. PXRD pattern of **POM**-800 composite after the HER test.

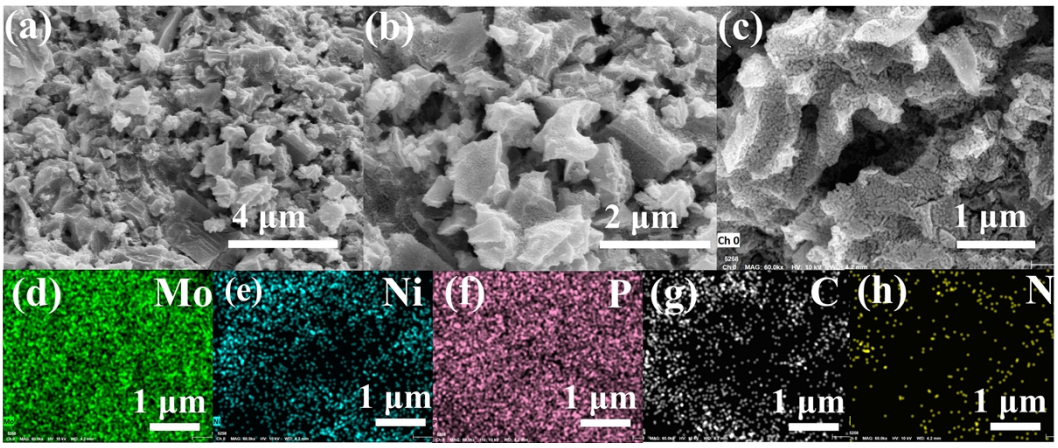

Fig. S9. (a-c) The SEM images of different magnifications and (d-h) the EDS mapping images of selected regions: Mo, Ni, N, P and C for **POM**-800 composite after HER test.

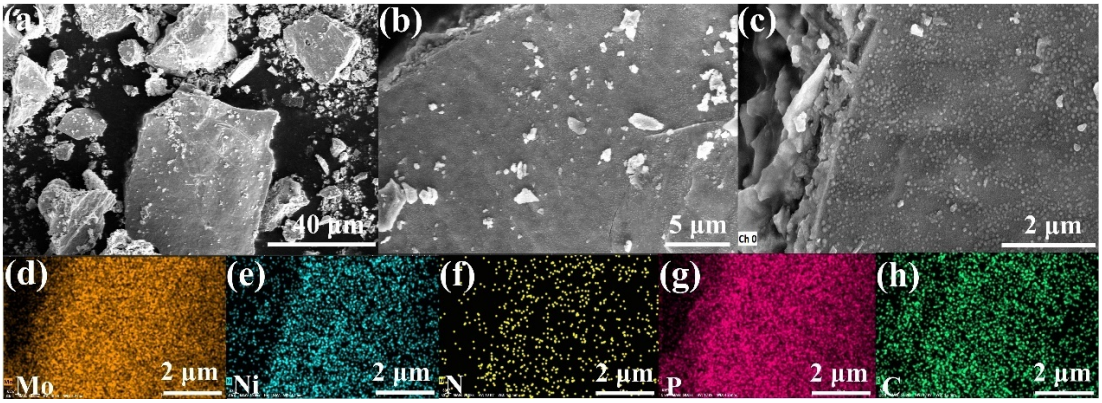

Fig. S10. (a-c) The SEM images of different magnifications and (d-h) the EDS mapping images of selected regions: Mo, Ni, N, P and C for **POM**-700 composite.

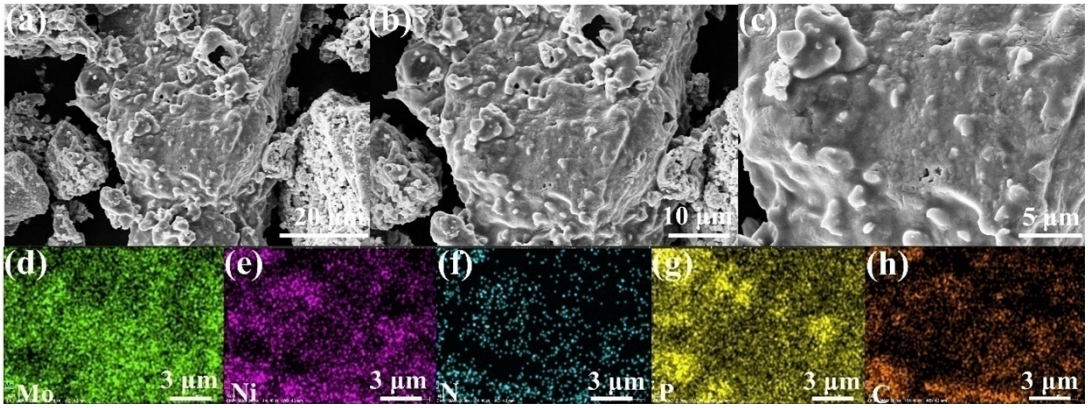

Fig. S11. (a-c) The SEM images of different magnifications and (d-h) the EDS mapping images of selected regions: Mo, Ni, N, P and C for **POM**-750 composite.

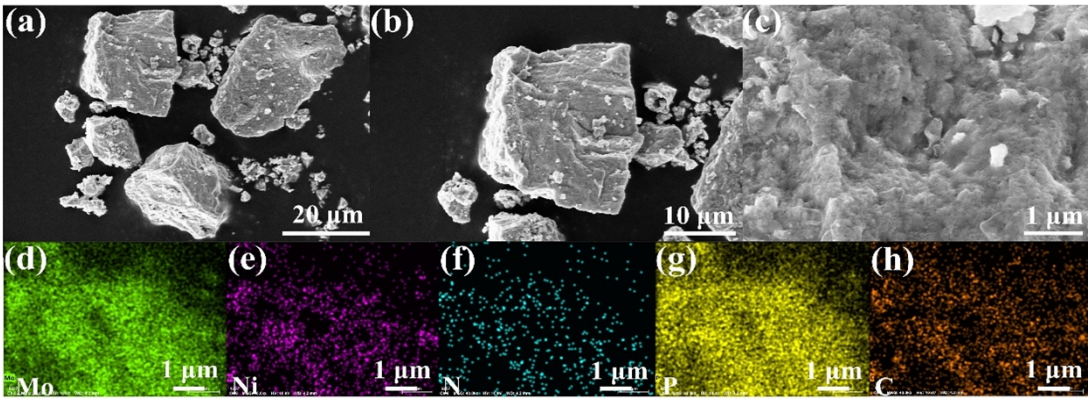

Fig. S12. (a-c) The SEM images of different magnifications and (d-h) the EDS mapping images of selected regions: Mo, Ni, N, P and C for **POM**-850 composite.

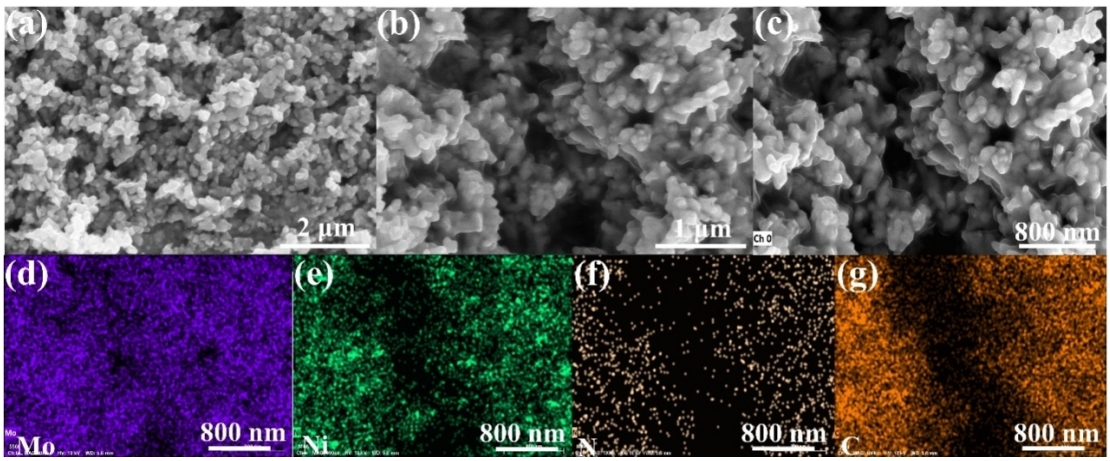

Fig. S13. (a-c) The SEM images of different magnifications and (d-h) the EDS mapping images of selected regions: Mo, Ni, N and C for **POM(S)**-800 composite.

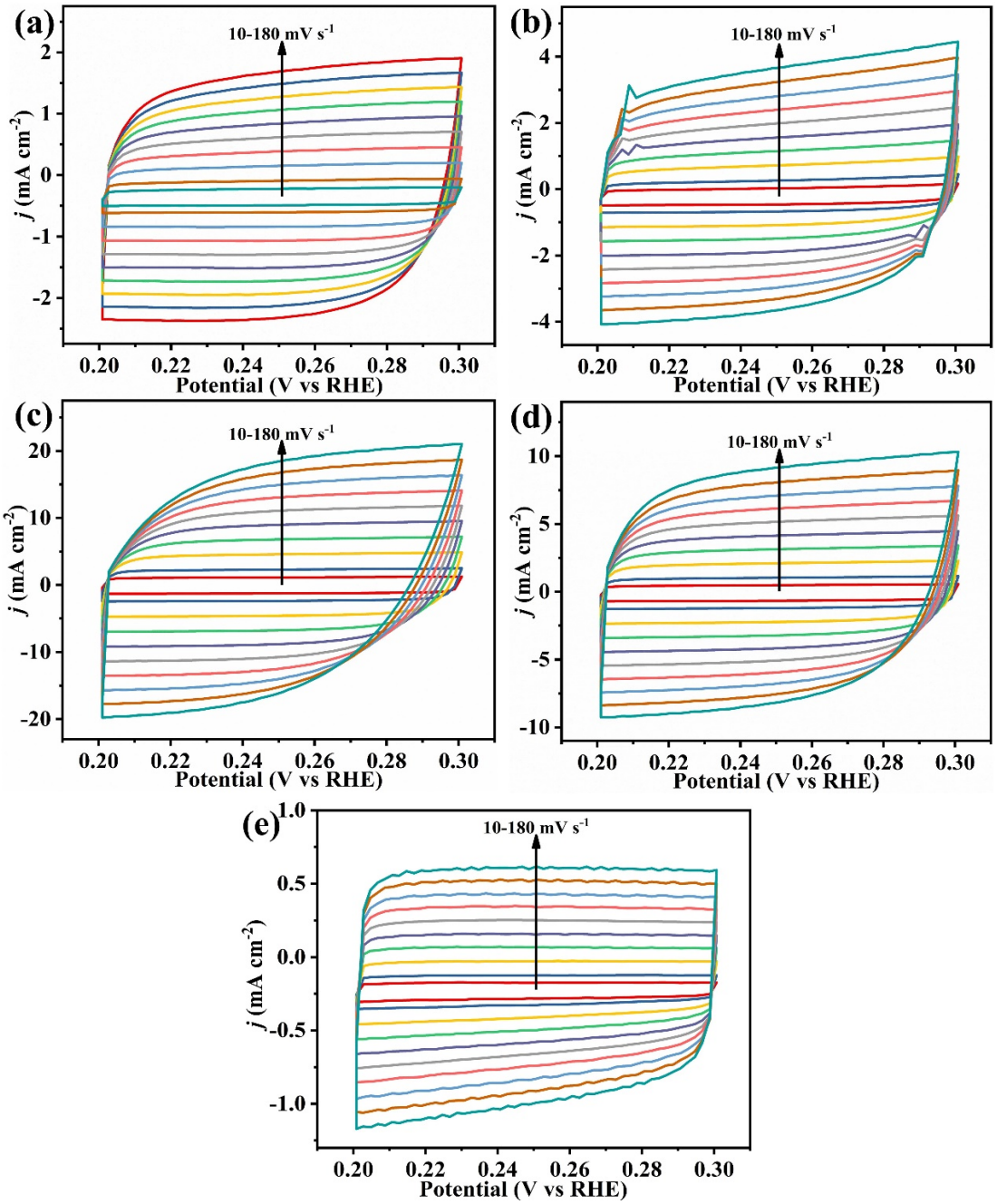

Fig. S14. CV curves of (a) **POM-700**. (b) **POM**-750. (c) **POM**-800. (d) **POM**-850 and (e) **POM(S)**-800 under capacitive region at scan rates from 10 to 180 mV s^{-1} in 1.0 M KOH.

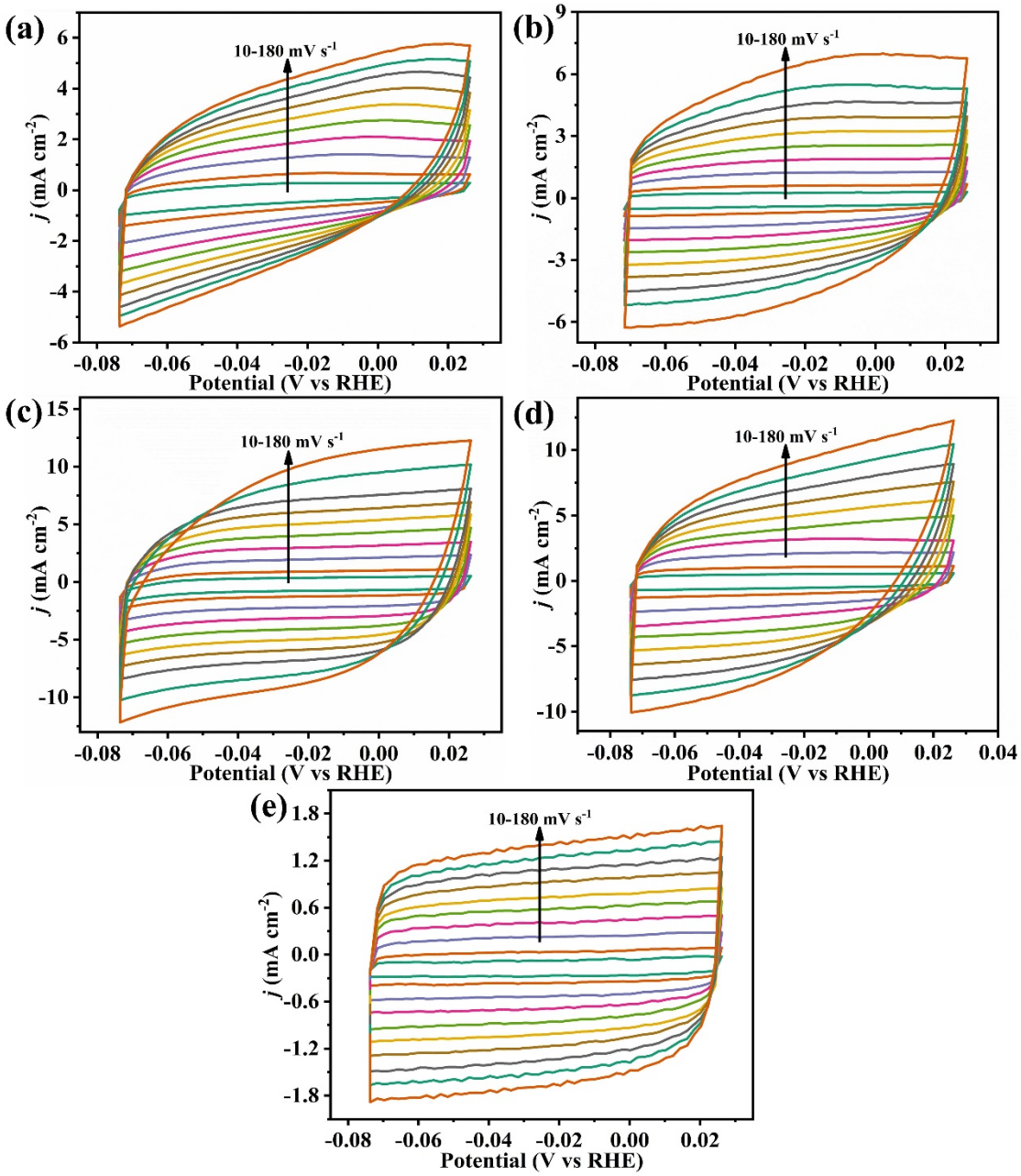

Fig. S15. CV curves of (a) **POM**-700. (b) **POM**-750. (c) **POM**-800. (d) **POM**-850 and (e) **POM(S)**-800 under capacitive region at scan rates from 10 to 180 mV s^{-1} in 0.5 M H_2SO_4.

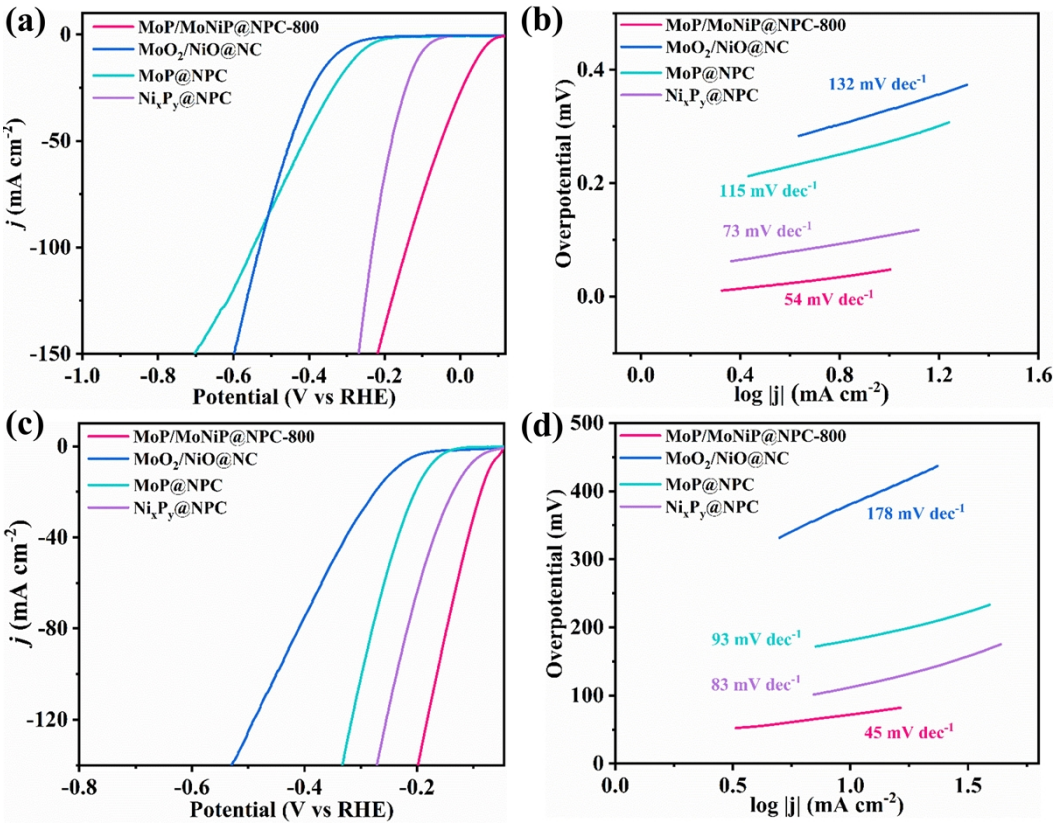

Fig. S16. (a,c) Polarization curves and (b,d) Tafel slopes calculated from LSV of **POM**-800, **POM(S)**-800, MoP@NPC and Ni_xP_y@NPC in 1.0 M KOH and 0.5 M H_2SO_4, respectively.

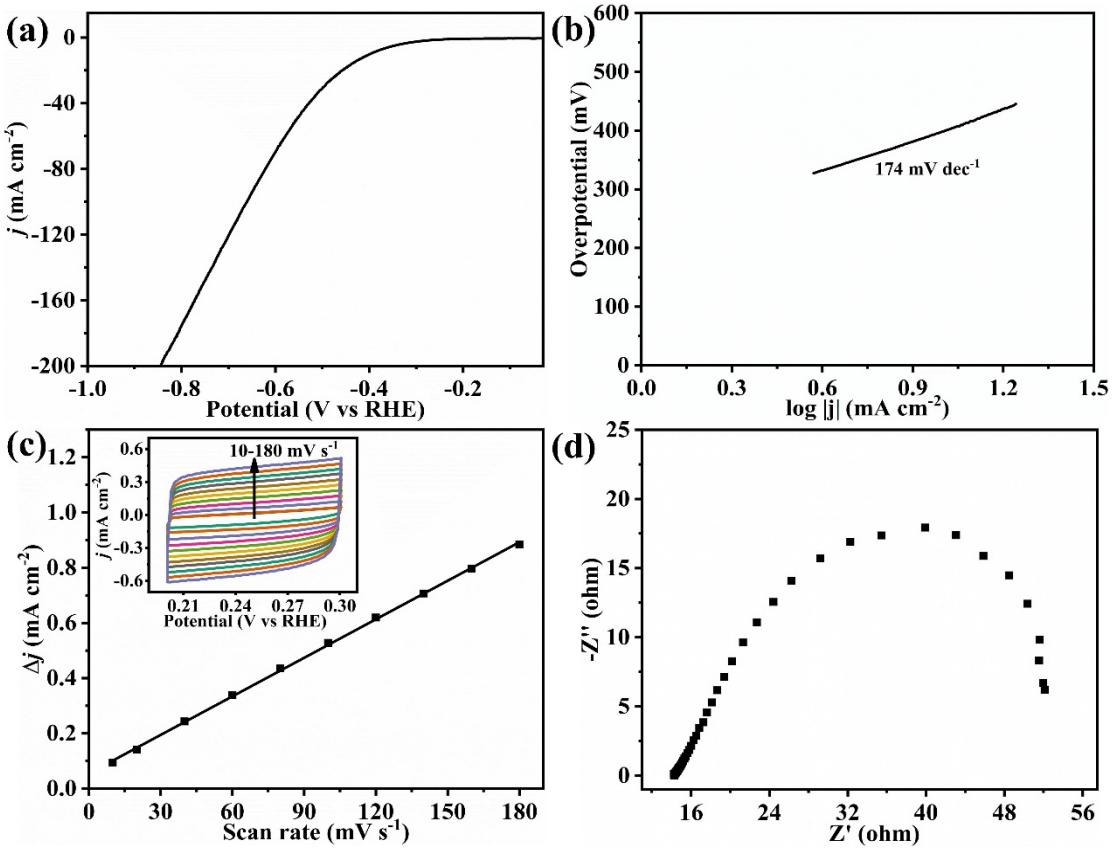

Fig. S17. (a) Polarization curve. (b) Tafel slope calculated from LSV. (c) The electrochemical C_{dl} linear fitting (inset: CV curves under capacitive region at scan rates from 10 to 180 mV s^{-1}) and (d) EIS spectra of **Ni-POM** catalyst in 1.0 M KOH.

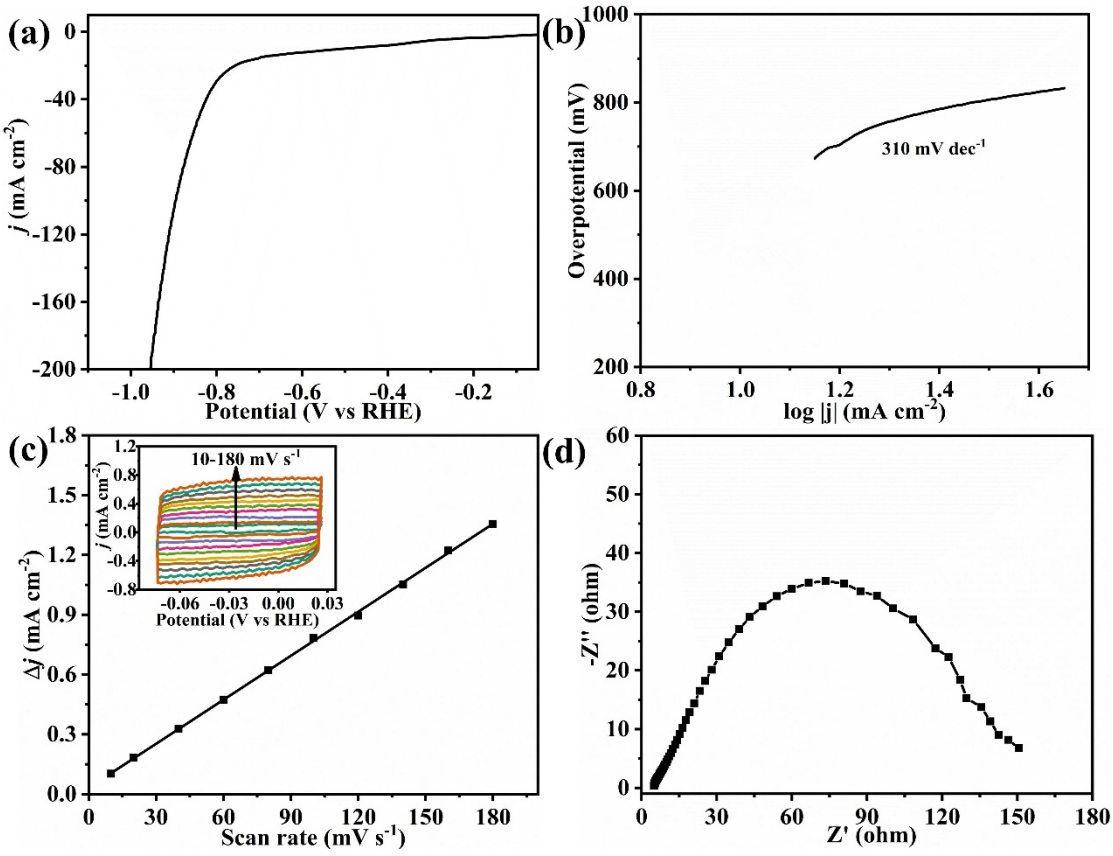

Fig. S18. (a) Polarization curve. (b) Tafel slope calculated from LSV. (c) The electrochemical C_{dl} linear fitting (inset: CV curves under capacitive region at scan rates from 10 to 180 mV s^{-1}) and (d) EIS spectra of **Ni-POM** catalyst in 0.5 M H_2SO_4.

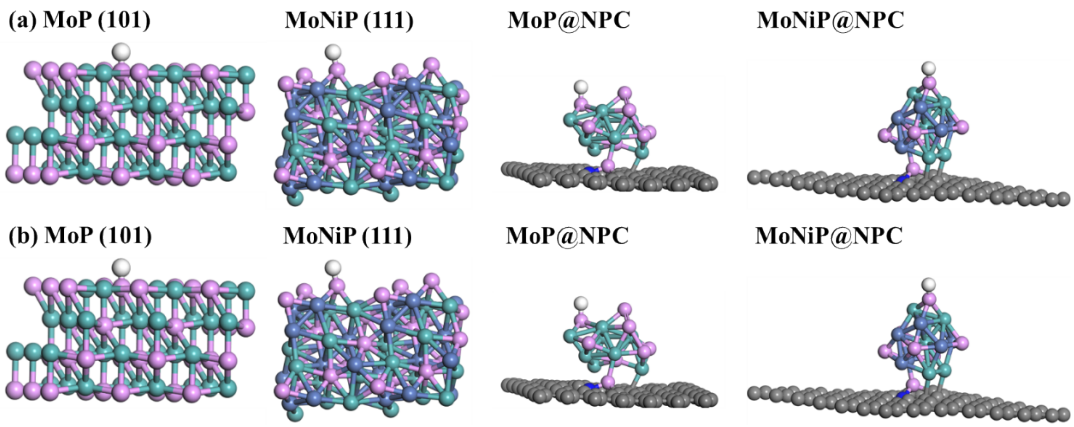

Fig. S19. (a) Geometry configurations of MoP (101), MoNiP (111), MoP@NPC and MoNiP@NPC. (b) The optimized H* adsorption structures on P atom in MoP (101), MoNiP (111), MoP@NPC and MoNiP@NPC.

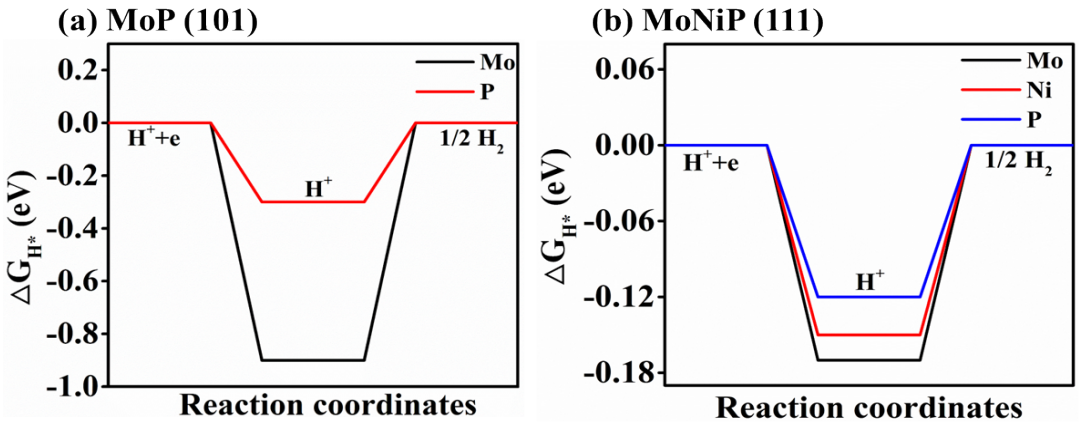

Fig. S20. DFT calculation results. Free-energy diagram for HER on (a) MoP (101) and (b) MoNiP (111).

S3. Additional Tables

Table S1. Crystal data and structure refinement parameters for **Ni-POM** precursor.

Compound	**[Ni(2,2'-bipy)$_3$][Mo$_6$O$_{19}$]**
CCDC	271878
Formula	$C_{30}H_{24}Mo_6N_6NiO_{19}$
F_w	1406.90
λ/Å	0.71073
T/K	298(2)
Crystal system	Monoclinic
Space group	$P2(1)/n$
a [Å]	12.2667(11)
b [Å]	18.8724(18)
c [Å]	17.1209(16)
α [°]	90
β [°]	101.326(3)
γ [°]	90
V (Å^3)	3886.3(6)
Z	4
D_c/Mg·m^{-3}	2.405
F(000)	2712
Reflections collected/unique	18718 / 6867
R_{int}	0.0700
Data/Restraints/Parameters	6867 / 0 / 559
R_1/wR_2 [$I>2\sigma(I)$] [a]	0.0521/0.1132
R_1/wR_2 [(all data)] [b]	0.0984/0.1376
GOF on F^2	1.097

[a] $R_1 = \Sigma(||F_0| - |F_C||)/\Sigma|F_0|$ [b] $wR_2 = [\Sigma w(|F_0|^2 - |F_C|^2)^2/(\Sigma w|F_0|^2)^2]^{1/2}$.

Table S2. Hydrogen-bonding geometry (Å, °) for **Ni-POM** precursor.

D*—H···*A	***D*—H**	**H···*A***	***D*···*A***	***D*—H···*A***
C_{13}—H_{11}···O_{12}	0.93	2.76	3.60	151
C_{17}—H_{13}···O_5	0.93	2.65	3.36	134
C_{29}—H_{18}···O_6	0.93	2.64	3.35	134
C_2—H_2···O_1	0.93	2.46	3.28	146
C_1—H_1···O_2	0.93	2.53	3.42	159
C_3—H_3···O_{10}	0.93	2.62	3.11	113
C_{23}—H_{22}···O_{12}	0.93	2.67	3.23	120
C_{14}—H_{12}···O_4	0.93	2.56	3.44	157
C_{30}—H_{17}···O_{17}	0.93	2.78	3.24	112
C_{18}—H_{14}···O_4	0.93	2.78	3.22	111

Symmetry codes: (i) -1/2+x, 3/2-y, 1/2+z; (ii) x, 1+y, 1+z; (iii) 3/2-x, 3/2+y, 5/2-z; (iv) 1-x, 2-y, 2-z; (v) x, 1+y, z; x, 2+y, z.

Table S3. Atomic percent of five **Ni-POM**-derived catalysts by SEM measurement.

Elemental composition (at %)						
Catalysts	**C**	**N**	**O**	**P**	**Mo**	**Ni**
POM-700	31.62	1.23	33.34	16.05	16.51	1.25
POM-750	15.39	1.95	54.80	12.05	14.13	1.68
POM-800	25.85	9.11	15.23	9.88	32.60	7.32
POM-850	19.88	0.94	16.19	29.96	32.52	0.51
POM(S)-800	14.24	1.74	60.61	--	22.91	0.51

Table S4. HER performance for transition metal-based phosphates.

Catalyst	Electrolyte	Overpotential (mV)η_{10}	Tafel slope (mV dec^{-1})	Stability	*Refs.*
MoP/MoNiP@NPC-800	**1.0 M KOH**	**50.4**	**54**	**1000 cycles 23 h**	**This work**
	0.5 M H_2SO_4	**72.6**	**74**	**2000 cycles 24 h**	
CoMoP@C	pH=2.2	204	80.54	1000 cycles 24 h	S6
	pH=14	81	55.53	1000 cycles 24 h	
MnP-MoP NPs/N,P-Gr	1.0 M KOH	74.2	57.7	26 h	S7
MoP/Fe_2P/RGO	1.0 M KOH	156	51	1000 cycles	S8
H-MoS_2/MoP	1.0 M KOH	92	59.8	30 h	S9
NM/rGO-2:1 (Ni-doped MoP/rGO-2:1)	1.0 M KOH	122	71.4	10 h	S10
Pt/Co_2P/Ni_2P/NF	1.0 M KOH	75	64	1000 cycles 25 h	S11
Ni_2P-MoP_2NRs/3D-NF	1.0 M KOH	82.2	52.9	20 h	S12
NiCoP@NF-100	1.0 M KOH	98	68	3000 cycles 24 h	S13
	0.5 M H_2SO_4	87	42	3000 cycles 24 h	
N-MoP/CC	1.0 M KOH	70	55	36 h	S14
MoP-NC	1.0 M KOH	131	66	1000 cycles	S15
Ni_2P/$Ni_{0.96}S$	1 M KOH with 0.5 M urea	72	151	20 h	S16

S4. References

S1 (a) G. M. Sheldrick, SHELXL97, Program for Crystal Structure Refinement; University of Göttingen: Göttingen, Germany, 1997; (b) G. M. Sheldrick, SHELXS97, Program for Crystal Structure Solution; University of Göttingen: Göttingen, Germany, 1997.

S2 G. Kresse and D. Joubert, From Ultrasoft Pseudopotentials to the Projector Augmented-Wave Method, *Phys. Rev. B*., 1999, **59**, 1758-1775.

S3 G. Kresse and J. Hafner, Molecular-Dynamics Simulation of the Liquid-Metal–Amorphous-Semiconductor Transition in Germanium, *Phys. Rev. B*, 1994, **49**, 14251-14269.

S4 G. Kresse and J. Furthmüller, Efficiency of Ab-Initio Total Energy Calculations for Metals and Semiconductors Using a Plane-Wave Basis Set, *Comput. Mater. Sci*., 1996, **6**, 15-50.

S5 J. P. Perdew, K. Burke and M. Ernzerhof, Generalized Gradient Approximation Made Simple, *Phys. Rev. Lett*., 1996, **77**, 3865-3868.

S6 Y. Y. Ma, C. X. Wu, X. J. Feng, H. Q. Tan, L. K. Yan, Y. Liu, Z. H. Kang, E. B. Wang and Y. G. Li, Highly Efficient Hydrogen Evolution from Seawater by a Low-Cost and Stable CoMoP@C Electrocatalyst Superior to Pt/C, *Energy Environ. Sci*., 2017, **10**, 788-798.

S7 C. D. Nguyen, V. H. Nguyen, Y. Vu-Thien, L. M. T. Pham and K. L. Vu-Huynh, Efficient and Stable Hybrid Electrocatalyst of Mixed MnP-MoP Nanoparticles–N,P-Codoped Graphene for Hydrogen Evolution Reaction, *Colloids Surf. A Physicochem. Eng. Asp*., 2020, **593**, 124609.

S8 K. W. Wang, J. S. Tan, Z. J. Lu, S. Chen, X. L. She, H. W. Zhang and D. J. Yang, Nanoscale Engineering MoP/Fe_2P/RGO Toward Efficient Electrocatalyst for Hydrogen Evolution Reaction, *Int. J. Hydrogen Energ*., 2018, **43**, 13939-13945.

S9 Q. Liu, Z. Q. Xue, B. Jia, Q. L. Liu, K. Liu, Y. Y. Lin, M. Liu, Y. L. Li and G. Q. Li, Hierarchical Nanorods of MoS_2/MoP Heterojunction for Efficient Electrocatalytic Hydrogen Evolution Reaction, *Small*, 2020, **16**, 2002482.

S10 L. Zhang, W. P. Xiao, Y. Zhang, F. Y. Han and X. F. Yang, Nanocarbon

Encapsulating Ni-doped MoP/Graphene Composites for Highly Improved Electrocatalytic Hydrogen Evolution Reaction, *Compos. Commun*., 2021, **26**, 100792.

S11 X. Xiao, D. P. Sun, X. C. Liu, B. Qiu, X. Y. Xu, D. E. Zhang and T. Yang, Ultra-low Amount Pt-doped Co_2P/Ni_2P on Nickel Foam as an Efficient Electrocatalyst for the Hydrogen Evolution Reaction in an Alkaline Electrolyte, *Sustain. Energ. Fuels*, 2021, **5**, 1059-1066.

S12 C. D. Nguyen, V. H. Nguyen and L. M. T. Pham, Three-dimensional $Ni_2P–MoP_2$ Mesoporous Nanorods Array as Self-standing Electrocatalyst for Highly Efficient Hydrogen Evolution, *Int. J. Hydrogen Energ*., 2020, **45**, 15063-15075.

S13 L. Chen, Y. H. Song, Y. Liu, L. Xu, J. Q. Qin, Y. P. Lei and Y. G. Tang, NiCoP Nanoleaves Array for Electrocatalytic Alkaline H_2 Evolution and Overall Water Splitting, *J. Energy Chem*., 2020, **50**, 395-401.

S14 M. Y. Fan, W. D. Wang, Y. Y. Zhu, X. Sun, F. W. Zhang and Z. P. Dong, Palladium Clusters Confined in Triazinyl-functionalized COFs with Enhanced Catalytic Activity, *Appl. Catal. B: Environ*., 2019, **257**, 117942.

S15 Y. Li, L. Cai, Q. L. Huang, J. Liu, R. R. Tang and W. H. Zhou, Highly Efficient Synthesis of Carbon-Based Molybdenum Phosphide Nanoparticles for Electrocatalytic Hydrogen Evolution, *Nanoscale Res. Lett*., 2020, **15**, 6.

S16 M. X. He, C. Q. Feng, T. Liao, S. N. Hu, H. M. Wu and Z. Q. Sun, Low-Cost $Ni_2P/Ni_{0.96}S$ Heterostructured Bifunctional Electrocatalyst toward Highly Efficient Overall Urea-Water Electrolysis, *ACS Appl. Mater. Interfaces*, 2020, **12**, 2225-2233.